Received: 5 April 2022 | Revised: 6 June 2022 | Accepted: 22 June 2022

DOI: 10.1002/jnr.25104

RESEARCH ARTICLE

JOURNAL OF Neuroscience Research

Plasticity of the spinal glymphatic system in male SD rats with painful diabetic neuropathy induced by type 2 diabetes mellitus

Guo-Qiang Wang[1,2] | Fei-Xiang Wang[1] | Yi-Na He[3] | Jing-Yan Lin[1]

[1]Department of Anesthesiology, the Affiliated Hospital of North Sichuan Medical College, Nanchong, China

[2]Department of Pain Treatment, Physical and Mental Hospital of Nanchong City, Nanchong, China

[3]Department of Anesthesiology, Nanchong Central Hospital, Nanchong, China

Correspondence
Jing-Yan Lin, Department of Anesthesiology, the Affiliated Hospital of North Sichuan Medical College, Nanchong, Sichuan, 637000, China.
Email: 419931094@qq.com

Funding information
the Affiliated Hospital of North Sichuan Medical College, Grant/Award Number: 2020ZD011

Abstract

The glymphatic system is a recently discovered glial-dependent macroscopic interstitial waste clearance system that promotes the efficient elimination of soluble proteins and metabolites from the central nervous system. Its anatomic foundation is the astrocytes and aquaporin-4 (AQP4) water channels on the endfeet of astrocytes. The aim of this study is to evaluate the plasticity of the spinal glymphatic system in male SD rats with painful diabetic neuropathy (PDN) induced by type 2 diabetes mellitus. PDN rats were modeled under a high-fat and high-glucose diet with a low dose of streptozotocin. MRI was applied to observe the infiltration and clearance of contrast to indicate the functional variability of the glymphatic system at the spinal cord level. The paw withdrawal threshold was used to represent mechanical allodynia. The numerical change of glial fibrillary acidic protein (GFAP) positive astrocytes was assessed and the polarity reversal of AQP4 protein was measured by immunofluorescence. As a result, deceased contrast infiltration and clearance, enhanced mechanical allodynia, increased number of GFAP positive astrocytes, and reversed polarity of AQP4 protein were found in the PDN rats. The above molecular level changes may contribute to the impairment of the spinal glymphatic system in PDN rats. This study revealed the molecular and functional variations of the spinal glymphatic system in PDN rats and for the first time indicated that there might be a correlation between the impaired spinal glymphatic system and PDN rats.

KEYWORDS
aquaporin-4, astrocyte, glymphatic system, painful diabetic neuropathy, polarity reversal, RRID:AB_10917109, RRID:AB_11006038, RRID:AB_2576208, RRID:AB_2722623, RRID:AB_2801330, RRID:AB_390192, RRID:MGI:5651135, RRID:SCR_003070, RRID:SCR_014570, RRID:SCR_016264, RRID:SCR_018949, RRID:SCR_019096, RRID:SCR_019961

1 | INTRODUCTION

Painful diabetic neuropathy (PDN) is one of the most common diabetic complications (Iqbal et al., 2018; Schmader, 2002; Schreiber et al., 2015), and is most often described as "burning," "electric," "sharp," and "dull/ache," which, for most, is worse at night time and when tired or stressed (Schmader, 2002). It affects the physical and mental health of patients seriously, leading to sleeping disorders, fatigue, and decreased activity, thus causing substantial interference in the enjoyment of life (Galer et al., 2000; Schmader, 2002). Owing to our limited knowledge of the underlying mechanism of PDN, current treatments are mainly focused on patients' symptoms and the therapeutic effects are unsatisfied (Iqbal et al., 2018;

Guo-Qiang Wang and Fei-Xiang Wang should be considered joint first author.

Edited by Junie Paula Warrington and Christopher Anderson. Reviewed by T. M. Zaved Waise and Mootaz M. Salman.

Javed et al., 2015). Studies have shown that a series of metabolic disorders occur in diabetic neuropathy (Hussain & Adrian, 2017). Hyperglycemia over activates the metabolic pathways, produces reactive oxidative species (ROS), activates pro-inflammatory transcription factors, and eventually promotes macrovascular and microvascular injury (Rendra et al., 2019). In addition, glutamate (excitatory neurotransmitter) clearance by astrocytes grown in high glucose is significantly impaired in the central nervous system (CNS) (Rivera-Aponte et al., 2015). The above abnormal metabolites might cause hyper-exciting of neurons in the CNS (central sensitization) thus leading to persistent pain sensation.

Waste removal is essential for maintaining homeostasis and the normal function of the CNS. The metabolic rate of the CNS is high, and synaptic transmission is sensitive to the changes in the surrounding environment. However, the CNS lacks authentic lymphatic vessels (Carare et al., 2014; Jessen et al., 2015). The glymphatic system is a recently discovered glial-dependent macroscopic interstitial waste clearance system that promotes the efficient elimination of soluble proteins and metabolites from the CNS, and its anatomic foundation is the astrocytes and aquaporin-4 (AQP4) water channels on the endfeet of astrocytes (Davoodi-Bojd et al., 2019; Iliff et al., 2013; Jessen et al., 2015). The impairment of the brain glymphatic system has been reported in neurodegenerative disorders, including Alzheimer's disease, traumatic brain injury, and cognitive deficiency associated with diabetes (Jiang et al., 2017; Kress et al., 2014; Peng et al., 2016).

Astrocytes, the most abundant type of glial cell, are accountable for sustaining homeostasis of the CNS. Studies have established that spinal astrocytes are activated in the pathology of PDN, such as increasing glial fibrillary acidic protein (GFAP), secretion of inflammatory cytokines, and adjusting the excitability of neurons and synaptic plasticity (Liao et al., 2010). Meanwhile, the function of the paravascular glymphatic pathway is facilitated by AQP4 water channels expressed in a highly polarized manor in astrocytic endfeet that ensheathe the vasculature in the CNS (Jessen et al., 2015; Plog & Nedergaard, 2018). Previous studies have demonstrated that the variation of localization of AQP4 is associated with CNS edema, and pharmacological inhibition of AQP-4 translocation to the blood–spinal cord barrier prevents the development of CNS edema and promotes functional recovery in injured rats (Kitchen et al., 2020; Salman, Kitchen, Halsey, et al., 2022; Sylvain et al., 2021). There are also studies that have indicated that astrocytes and AQP4 water channels are involved in the maintenance of chronic pain (Lu, Pang, et al., 2020; Mai et al., 2021). Besides, it is noteworthy that the cellular composition of the spinal cord is similar to that of the brain, and many other studies have shown that the glymphatic system also exists in the spinal cord (Benveniste et al., 2017; Liu et al., 2018; Wei et al., 2017). Taken as a whole, these pieces of evidence suggest that there might exist molecular and functional variations of the spinal glymphatic system in PDN rats.

In this study, we established a rat model of PDN, and due to a certain degree of difficulty in obtaining and using the more rapid and extensive tracer, such as H217O tracer, we used the classic MRI tracer, the Gadolinium-diethylenetriamine Penta-acetic acid (Gd-DTPA), to investigate the functional variations of paracellular flow of the spinal glymphatic system (Alshuhri et al., 2021; Salman et al., 2021). The paw withdrawal threshold was used to represent mechanical allodynia. Furthermore, the numerical change in GFAP-positive astrocytes and polarity reversal of AQP4 protein were measured. The present study lays the foundation for the mechanism of PDN and provides a possible therapeutic target.

Significance

The glymphatic system is a recently discovered glial-dependent macroscopic interstitial waste clearance system that promotes the efficient elimination of soluble proteins and metabolites from the central nervous system. The impairment of the glymphatic system had been reported in neurodegenerative disorders. This study revealed the molecular and functional variations of the spinal glymphatic system in rats with painful diabetic neuropathy (PDN) and for the first time proved that PDN was significantly correlated with the impairment of the spinal glymphatic system. The present study provides new views into the pathogenesis and possible therapeutic targets of PDN.

2 | MATERIALS AND METHODS

2.1 | Animal husbandry

Male adult Sprague–Dawley rats (n = 25, bodyweight 160–180 g, 5–6 weeks, RRID:MGI:5651135) were obtained from the laboratory animal center of North Sichuan Medical College and were housed one per cage. Rats were fed under a 12/12 h light/dark cycle at a room temperature of 21–23°C and with food and water available ad libitum.

The rats were randomly allocated into the control group (Group C, n = 10, fed with a normal diet, 57% carbohydrate, 22% protein, 6% fat, 8% cellulose, and 7% other elements) and the PDN modeling group (Group PDN, n = 15, fed with a high-fat and high-glucose diet, 60% normal fodder, 20% sucrose, 15% axunge and 5% cholesterol) (Lin et al., 2018). The feed, water intake, and urination of all rats were observed and recorded every day.

2.2 | PDN model husbandry

At present, the mainstream modeling method of type 2 diabetes model was to induce insulin resistance through a 'high-fat and high-glucose' diet, and then injected with a small dose of STZ to destroy islet β cells, and finally simulated the pathogenesis process of human type 2 diabetes as much as possible (Huang et al., 2020;

Lin et al., 2018; Liu et al., 2019; Zhang et al., 2020). Therefore, slight differences in the high-fat and high-glucose diet composition used by different researchers were allowed. Since we were not familiar with the modeling process of other references, the diet and modeling process was based on our previous study (Lin et al., 2018). In brief, after feeding according to the experimental protocol for 5 weeks, rats in Group PDN were intraperitoneally injected with 1% streptozotocin (STZ, 25 mg/kg, sigma chemical, USA) while rats in Group C were injected with an equal volume of sterile saline. The fasting blood glucose (FBG) was measured 72 h after STZ injection using a one-touch glucometer and matched glucose strips (Johnsons & Johnsons, New Jersey, USA). Rats with FBG above 16.7 mmol/L were considered type 2 diabetes mellitus (T2DM).

2.3 | Behavioral tests

The paw withdrawal threshold (PWT), tested by VonFrey filaments kit with pressure ranging from 0.008 to 180 g (US PAT. 5823969 8512259, North Coast, California, USA), was used to represent tactile allodynia and mechanical hyperalgesia. The PWT was measured every 7 days after the FBG was tested. It was calculated by the "up–down" method as we described previously (Lin et al., 2017; Mei et al., 2011; Peng et al., 2010): the VonFrey filaments were applied perpendicularly to the hind paw with increasing pressures to induce a positive withdrawal response. Each pressure lasted for 6–8 s for avoiding possible injury to the hind paw and was repeated four times at different sites of the hind paw. If one positive response was induced, then two additional stimulations at that pressure were applied to the hind paw. The pressure which could induce three times withdrawal responses in six stimulations was recorded as the PWT. The PWT measurements were carried out by the same investigators from 9 to 11 am on experimental days in the same room.

Three weeks after the measurement of FBG, there were a total of 11 rats in the Group PDN that manifested increased FBG, decreased PWT and polydipsia, polyuria, and polyphagia, these rats were considered successfully modeled as PDN rats. Finally, there were 10 rats in Group C and 11 rats in the Group PDN used for further research, respectively.

2.4 | MRI measurement

Just at the time when the significant decrease in PWT was observed (3 weeks after measurement of FBG), five rats in each group were randomly selected for MRI measurement. All rats were anesthetized using a small animal anesthesia machine (MIDMARK Matrx VMR, USA). Anesthesia was inducted using oxygen (1.7 L/min) with isoflurane (5%) for 5 min and maintained using oxygen (1.7 L/min) with isoflurane (1.0%–2%) (Albargothy et al., 2018). Each rat was placed prone on the operating table and the lower abdomen was raised. A blunt protrusion in the lower part of the spine was the hip nodule, and its horizontal position was the lumbar 6 vertebrae. After skin preparation, disinfection, and covering gauze, a glass capillary micropipette with an adjusted diameter (Sigma, UK) was advanced gently to pass through the lumbar 4/5 intervertebral space until tail flutter or sudden lateral sway indicated entry into the spinal subarachnoid space (Xu et al., 2006; Zhong-Xian et al., 2004). A total of 25 μl of diluted Gd-DTPA (100 μl Gd-DTPA was diluted with 900 μl sterile saline) was injected into the L4/5 subarachnoid space at a constant rate (1 min). The capillary micropipette was left in situ for 3 min to prevent reflux (Lam et al., 2017). All rats were transferred to an MRI rat special coil for MRI scanning after withdrawal of the capillary micropipette.

MRI scan was obtained using a GE 3.0T (Discovery MR750, GE, USA, RRID:SCR_019961) magnetic resonance scanner with an eight-channel rat special coil. Rats were placed prone in the coil. Heart rate and rectal temperature were continuously monitored. Isoflurane concentration was adjusted as necessary so that the righting reflex disappeared, no retraction of paws under pressure, and the heart rate was maintained at 328 ± 10 beats per minute. Rectal temperature was maintained at 37 ± 0.5°C using a feedback-controlled air heating blower (Rapid Electric, Brewster, NY, USA) (Wood et al., 2001). T1-weighted MRI (T1WI) was used for scanning the lumbar enlargement of the spinal cord before Gd-DTPA injection and for 15 min, 30 min, 1, 1.5, 2, 2.5, 3, and 6 h after Gd-DTPA injection and the inflowing into and draining out of the contrast agent to the spinal cord were observed. The fast spin-echo (FSE) sequence was used for axial T1WI scanning. The parameters were as follows: TR: 575 ms, MinTE: 9.5 ms, MaxTE: 28.4 ms, Slice thickness: 3.0 mm, Slice space: 0.0 mm: FOV: 7.0 × 7.0 cm, Matrix: 288 × 256, Flip angle: 142, Bandwidth: 31.25 kHz, NEX: 3.

At each time point described above, a typical picture of the lumbar enlargement was selected. The MRI signal intensity (SI) of the ventral horn, the dorsal horn, and the central canal on each selected picture were measured at the same region of interest (ROI, area was 0.5 mm^2). The average of the five results on each picture was recorded as the SI of the picture.

2.5 | Number of astrocytes

2.5.1 | Tissue blocks and section

The number estimation of GFAP positive astrocytes was administered 4 weeks after measurement of FBG due to the long duration of MRI scanning. The last five rats in the Group C and six rats in Group PDN were applied to the stereological study of astrocytic numbers.

Rats were anesthetized with 50 mg/kg of 10% chloral hydrate intraperitoneally. Then the transcardiac perfusion with 200 ml of sterile normal saline followed by 200 ml of 4% paraformaldehyde in 0.1 M phosphate-buffered saline (PBS, PH 7.4) was administered. Afterward, the L5 lumbar cord segment was dissected according to the positions of the spinal nerve roots (Lin et al., 2018).

The L5 lumbar cord segments were post-fixed in 4% paraformaldehyde for 2 days, then embedded in paraffin (Histowax; Leica Instrumental Ltd, Shanghai, China). Afterward, tissue blocks were sectioned in the direction perpendicular to the long axis of the spinal cord with a thickness of 14 μm and three sections were sampled from 15 serial sections according to a systematic (equal spaced) manner.

2.5.2 | Immunohistochemistry

The GFAP was applied for immunohistochemistry staining. A commercial kit (Beijing Zhongshan Golden Bridge Biotechnology Co., Ltd., Beijing, China) was used for immunostaining according to the instructions of the producer. Sections were deparaffinized and handled sequentially as follows: (1) boiled for 15 min in the citrate buffer (pH 6.0) for antigen retrieval, (2) incubated with 3% hydrogen peroxide for 10 min to block endogenous peroxidase activity, (3) incubated with mouse anti-GFAP monoclonal antibody (diluted at 1:500 in PBS containing 0.3% Triton X-100, MAB3402B, Millipore, Massachusetts, USA, RRID:AB_10917109) at 4°C for 50 h, (4) incubated with goat anti-mouse IgG conjugated to horseradish peroxidase (HRP) (diluted at 1:500 in PBS, 12-349, Millipore, Massachusetts, USA, RRID:AB_390192) for detecting GFAP, (5) bound HRP was detected with 3,3-diaminobenzidine (DAB), and (6) counterstained with hematoxylin. The specificity of the GFAP antibody was validated by immunofluorescence assay on brain sections of the GFAP$^{-/-}$ mouse (Iorio et al., 2018) (Table 1).

2.5.3 | Stereological measurements

To implement the blinded manner, all sections were numbered and the observation side (left or right, alternately chosen) was marked by the designer first. The sections were observed and measured under the NewCAST stereology set (Visiopharm, Hørsholm, Denmark, RRID:SCR_014570) matched with an Olympus BX51 light microscope (Olympus, Tokyo, Japan, RRID:SCR_018949).

The procedure for estimating the number of GFAP-positive astrocytes was the same as the estimation of synaptic numbers which we described in the previous studies (Lin et al., 2018; Peng et al., 2010).

TABLE 1 The primary and secondary antibodies used

Antibody name	The exact structure of the immunogen against which the animal was immunized	Manufacturer/catalog number/RRID/host species/clonality	Concentration used
Anti-GFAP	MERRRITSAARRSYVSSGEMMVGGLAPGRRLGPGTRLSLARMPP PLPTRVDFSLAGALNAGFKETRASERAEMMELNDRFASYIEKVRFLEQQNKALAAELN QLRAKEPTKLADVYQAELRELRLRLDQLTANSARLEVERDNLAQDLATVRQKLQDETN LRLEAENNLAAYRQEADEATLARLDLERKIESLEEEIRFLRKIHEEEVRELQEQLARQ QVHVELDVAKPDLTAALKEIRTQYEAMASSNMHEAEEWYRSKFADLTDAAARNAELLR QAKHEANDYRRQLQSLTCDLESLRGTNESLERQMREQEERHVREAASYQEALARLEEE GQSLKDEMARHLQEYQDLLNVKLALDIEIATYRKLLEGEENRITIPVQTFSNLQIRET SLDTKSVSEGHLKRNIVVKTVEMRDGEVIKESKQEHKDVM	Millipore/MAB3402B/RRID:AB_10917109/Mouse/Monoclonal	1/500
Goat anti-mouse IgG	Goat anti-mouse peroxidase conjugate immunoglobulins heavy and light chains	Millipore/12-349/RRID:AB_390192/Goat/Polyclonal	1/500
Anti-AQP4	MSDRPTARRWGKCGPLCTRENIMVAFKGVWTQAFWKAVTAEFLA MLIFVLLSLGSTINWGGTEKPLPVDMVLISLCFGLSIATMVQCFGHISGGHINPAVTV AMVCTRKISIAKSVFYIAAQCLGAIIGAGILYLVTPPSVVGGLGVTMVHGNLTAGHGL LVELIITFQLVFTIFASCDSKRTDVTGSIALAIGFSVAIGHLFAINYTGASMNPARSF GPAVIMGNWENHWIYWVGPIIGAVLAGGLYEYVFCPDVEFKRRFKEAFSKAAQQTKGS YMEVEDNRSQVETDDLILKPGVVHVIDVDRGEEKKGKDQSGEVLSSV	Novus/NBP1-87679/RRID:AB_11006038/Rabbit/Polyclonal	1/150
Anti-CD31	MQPRWAQGATMWLGVLLTLLLCSSLEGQENSFTINSVDMKSLPD WTVQNGKNLTLQCFADVSTTSHVKPQHQMLFYKDDVLFYNISSMKSTESYFIPEVRIY DSGTYKCTVIVNNKEKTTAEYQVLVEGVPSPRVTLDKKEAIQGGIVRVNCSVPEEKAP IHFTIEKLELNEKMVKLKREKNSRDQNFVILEFPVEEQDRVLSFRCQARIISGIHMQT SESTKSELVTVTESFSTPKFHISPTGMIMEGAQLHIKCTIQVTHLAQEFPEIIIQKDK AIVAHNRHGNKAVYSVMAMVEHSGNYTCKVESSRISKVSSIVVNITELFSKPELESSF THLDQGERLNLSCSIPGAPPANFTIQKEDTIVSQTQDFTKIASKSDSGTYICTAGIDK VVKKSNTVQIVVCEMLSQPRISYDAQFEVIKGQTIEVRCESISGTLPISYQLLKTSKV LENSTKNSNDPAVFKDNPTEDVEYQCVADNCHSHAKMLSEVLRVKVIAPVDEVQISIL SSKVVESGEDIVLQCAVNEGSGPITYKFYREKEGKPFYQMTSNATQAFWTKQKASKEQ EGEYYCTAFNRANHASSVPRSKILTVRVILAPWKKGLIAVVIIGVIIALLIIAAKCYF LRKAKAKQMPVEMSRPAVPLLNSNNEKMSDPNMEANSHYGHNDDVRNHAM KPINDNKE PLNSDVQYTEVQVSSAESHKDLGKKDTETVYSEVRKAVPDAVESRYSR TEGSLDGT	Santa Cruz/sc-376764/RRID:AB_2801330/Mouse/Monoclonal	1/50
Alexa Fluor 488	Goat anti-mouse gamma immunoglobulins heavy and light chains	Abcam/ab150113/RRID:AB_2576208/Goat/Polyclonal	1/500
Alexa Fluor 647	Goat anti-rabbit gamma immunoglobulins heavy and light chains	Abcam/ab150079/RRID:AB_2722623/Goat/Polyclonal	1/500

In brief, the region of the spinal dorsal horn was delineated, and its cross-sectional area (A) was estimated using a × 10 objective lens first.

Then, a 100× oil immersion lens with a numerical aperture of 1.40 was administrated to observe the delineated region, the final magnification on the computer screen was 2240×. All testing fields were sampled according to a systematical manner (equally spaced 0.15 mm) with a motorized stage until the whole delineated region was sampled completely. The first testing field was randomly determined from the upper left corner in the delineated region. On each field, two rectangular frames (each with an area of 1882.5 μm^2) were superimposed.

In counting GFAP-positive astrocytes, the upper surface of the section was first brought into focus in each field, and then the section was observed by manually focusing down. To avoid possible imperfections, the first 0.5 μm of optical sections were discarded for counting. The next 7 μm of serial optical sections (i.e., the volume of each optical disector was 1882.5 × 7 = 13,177.5 μm^3) were used for counting according to the disector counting rule (Gundersen et al., 1988; Lin et al., 2018): when a new GFAP-positive astrocyte came into focus 'within' the counting frame, that GFAP-positive astrocyte was counted. In this study, an average of 60 fields was sampled and an average of 387 GFAP-positive astrocytes was counted on the selected side of the L5 spinal cord per animal.

The numerical density of GFAP-positive astrocytes (Nv, number per volume) in the spinal dorsal horn was calculated with the total number of GFAP-positive astrocytes counted and the total volume of disectors used.

In consideration of not knowing the precise boundary of the L5 segment of the spinal cord, we applied the number of GFAP-positive astrocytes in 1 mm length of the L5 spinal dorsal horn to represent the numerical data of the whole L5 segment. The total number of GFAP-positive astrocytes in 1 mm length of the spinal dorsal horn (NH) was calculated by multiplying Nv by the volume of 1 mm length of the spinal dorsal (A × 1 mm). Considering that the length of the spinal cord was compressed during tissue processing and section preparation, the total number of GFAP-positive astrocytes in 1 mm length of the fresh spinal dorsal horn was obtained by multiplying NH by the coefficient of compression (Jing-Yan et al., 2010). In the present study, we only counted GFAP-positive astrocytes for the reason that reactive astrocytes increase the production of GFAP and therefore are more easily counted by the immunostaining techniques. The actual numerical variation of astrocytes in the spinal cord of PDN rats needs further study.

2.6 | Immunofluorescence

The section production process was the same as above, except the thickness of the slices changed from 14 to 4 μm. Deparaffinize and rehydrate tissue sections using standard methods. After deparaffinization and rehydration, sections were managed sequentially as follows: (1) boiled in the citrate buffer (pH 6.0) for 20 min for antigen retrieval, (2) blocked with 5% normal goat serum for 60 min, (3) incubated with AQP4 antibody (1:150, Novus, NBP1-87679, Shanghai, China, RRID:AB_11006038) and PECAM-1/CD31 antibody(1:50, Santa Cruz, sc-376764, Texas, USA, RRID:AB_2801330) at 4°C overnight, (4) rewarmed at 37°C for 30 min and washed 3 times with PBS buffer (15 min each), (5) incubated with secondary goat anti-rabbit IgG H&L antibodies (1:500, Abcam, ab150079, Cambridge, UK, RRID:AB_2722623) and goat anti-mouse IgG H&L antibodies (1:500, Abcam, ab150113, Cambridge, UK, RRID:AB_2576208) at 37°C and protected from light for 2 h and rinsed 3 times with PBS buffer (15 min each), and (6) sealed with Anti-fluorescence quenching sealing solution with DAPI (Beyotime, p0131, Shanghai, China). Finally, the section was mounted and observed under an Olympus FV1200 confocal laser scanning microscope (RRID:SCR_016264) with a 40× objective lens. The parameters were as follows: DAPI: HV 477, Gain 2, Offset 22; Alexa Fluor 488: HV 555, Gain 1, Offset 59; Alexa Fluor 647: HV 466, Gain 1, Offset 38. The typical images were selected to indicate the polarity reversal of AQP4 protein.

2.7 | Quantification of AQP4 polarization

A total of three randomly selected sections/animal in each group were analyzed in a blinded manner by investigators blinded to treatment conditions using ImageJ version 1.53e bundled with Java 1.8.0_172 software (National Institutes of Health, RRID:SCR_003070). For an unbiased representation of the images, all laser power parameters, pinhole size, and image detection were kept constant for all samples. To avoid the influence of nonspecific staining motor neurons on measurement, the perivascular region was defined as being CD31 positive, having a complete cross section of blood vessels and no surrounding dendrites. Briefly, perivascular polarization of AQP4 was measured as follows: (1) split channels of the images, (2) chose the AQP4 channel image and set the threshold automatically, (3) measured the median immunofluorescence intensity of perivascular regions, and (4) applied the threshold analysis to measure the percentage of the region exhibiting AQP4 immunofluorescence greater than or equal to perivascular AQP4 immunofluorescence of the total field of view. Finally, AQP4 polarization was expressed as the percentage of the region that exhibited lower AQP4 immunofluorescence than the perivascular regions (Harrison et al., 2020).

2.8 | Statistical analysis

Statistical analyses were performed using the SPSS software version 19 (IBM Corporation, Armonk, NY, RRID:SCR_019096). All values were shown as mean ± SD. The one-way analysis of variance (ANOVA) was used to compare means between groups. The repeated-measures ANOVA was used to compare the body

weight, glucose, PWT, and MRI signal intensity. Significance was set at $p < .05$.

3 | RESULTS

3.1 | Bodyweight, blood glucose, and PWT in each group of rats

As shown in Figure 1, the body weight (compared with values in group C, $F = 6.74$, $n = 21$, $p = .002$; compared with values of pre-injection, $F = 6.21$, $n = 11$, $p = .04$) decreased significantly while the blood glucose (compared with values in group C, $F = 102.14$, $n = 21$, $p < .001$; compared with values of pre-injection, $F = 404.40$, $n = 11$, $p < .001$) increased significantly after STZ intraperitoneal injection in the Group PDN when compared with values of pre-injection or values in Group C, which indicated the modeling process of diabetic rats was successfully completed. Compared to Group C, the PWT decreased significantly in the PDN group 21 days after the measurement of FBG and lasted until the end of the experiment ($F = 3.93$, $n = 21$, $p = .02$). The PWT decreased significantly in the Group PDN at 21 days after measurement of FBG compared with values of pre-injection ($F = 15.70$, $n = 11$, $p = .004$).

3.2 | MRI imaging

3.2.1 | Dynamic observation of Gd-DTPA inflowing into and draining out of the spinal cord

The SI of the lumbar enlargement of the spinal cord changed dynamically with time. Before Gd-DTPA injection, there was no contrast agent signal in lumbar enlargement in each group. Fifteen minutes after Gd-DTPA injection, the contrast agent was discontinuously distributed on the surface of the pia mater. As time went by, the contrast agent inflowed into the ventral horn and the dorsal horn along the anterior lateral sulcus or the posterior lateral sulcus ("four-horn sign"). When the contrast agent reached its peak, the gray matter appeared the brightest "butterfly shape," and then gradually darkened. There was no contrast agent signal in white matter in each group after Gd-DTPA injection (Figure 2).

3.2.2 | Measurement results of SI

Before injection of Gd-DTPA, there was no significant difference between groups in terms of the SI in the lumbar enlargement ($F = 0.01$, $n = 10$, $p = .93$). Compared to Group C, the peak of SI (PEAK SI)

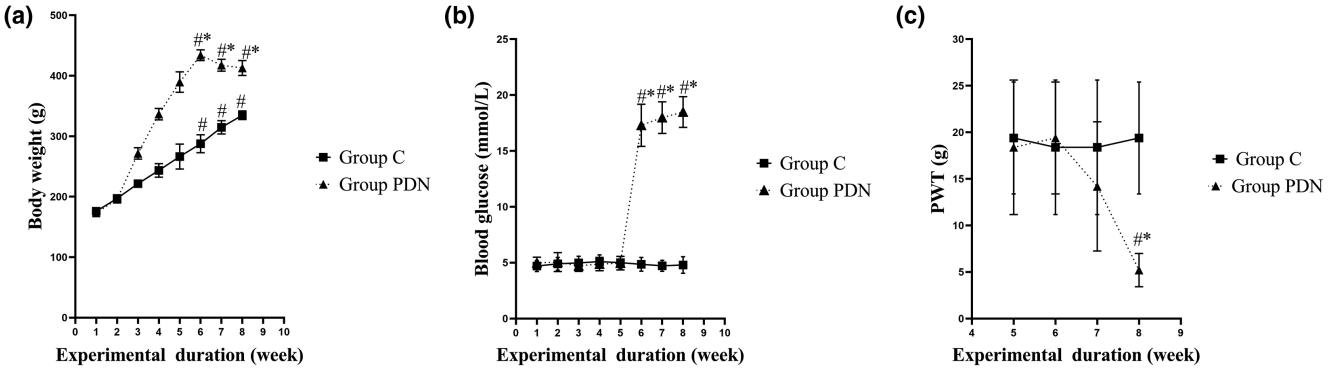

FIGURE 1 Trend of body weight, blood glucose, and paw withdrawal threshold (PWT) in each group. (a) The trend of body weight in group C and group PDN. (b) The trend of blood glucose in group C and group PDN. (c) The trend of PWT in group C and group PDN. The intraperitoneal injection of sterile saline (group C, $n = 10$) or streptozotocin (STZ, 25 mg/kg, group PDN, $n = 11$) was administrated at the 5th week of feeding. Values were presented as mean ± SD. $^{*}p < .05$ compared with values in group C. $^{\#}p < .05$ compared with values of pre-injection in each group.

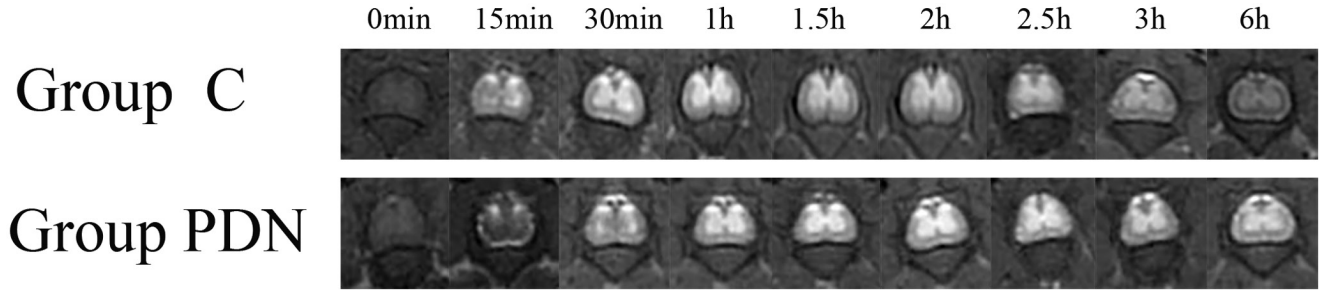

FIGURE 2 The MRI image with time in lumbar enlargement of the spinal cord of rats in the group C and group PDN before and after 25 μl diluted gadolinium-diethylenetriamine Penta-acetic acid (Gd-DTPA, 100 μl Gd-DTPA was diluted with 900 μl sterile saline) injection (0 min–6 h) through the lumbar 4/5 intervertebral space. See Figure 1 for the meaning of the grouping abbreviation.

showed no significant difference in the Group PDN ($F = 2.16$, $n = 10$, $p = .18$), the time to reach PEAK SI (PEAK SI TIME) was delayed significantly in the Group PDN ($F = 49.84$, $n = 10$, $p < .001$), the SI in the lumbar enlargement 6 h after finishing Gd-DTPA injection (SIX-HOUR SI) was higher in the Group PDN ($F = 230.13$, $n = 10$, $p < .001$), the variation of the SI per hour after SI reached its peak (SIPH) decreased significantly in the Group PDN ($F = 146.41$, $n = 10$, $p < .001$) (Table 2).

3.3 | Number of GFAP-positive astrocytes in the rat spinal dorsal horn

The area of the spinal dorsal horn had no significant difference between the two groups ($F = 0.05$, $n = 11$, $p = .82$). The number of GFAP-positive astrocytes per mm length of the L5 spinal dorsal horn increased significantly in the Group PDN compared with Group C ($F = 12.18$, $n = 11$, $p = .01$) (Figure 3, Table 3).

3.4 | Polarity localization of AQP4 protein

To verify the polarity reversal of AQP4 protein, we examined the localization of AQP4 protein by immunofluorescence staining with the additional vascular endothelial cell markers CD31 (Stokum et al., 2015). As shown in Figure 4 and Table 3, the reduced perivascular localization of AQP4 protein of rats in Group PDN was concordant with a reduction of "polarization" of this water channel to blood vessels [AQP4 'polarization' of rats in Group C, 66.87% (±6.90%) versus 34.61% (±6.99%) of rats in Group PDN], which indicated the polarity reversal of AQP4 protein in Group PDN ($F = 58.83$, $n = 11$, $p < .001$).

4 | DISCUSSION

This is the first study determining the functional and structural variation of the spinal glymphatic system in rats with PDN induced by type 2 diabetes mellitus. As demonstrated, the manifestation of rats

TABLE 2 MRI signal intensity (SI) obtained from the lumbar enlargement

	Group C ($n = 5$)	Group PDN ($n = 5$)	p-value
Pre-injection	2188.80 ± 40.52	2191.60 ± 61.18	.93
PEAK SI[a]	7014.40 ± 80.97	7076.40 ± 48.37	.18
SIX-HOUR SI[b]	4571.80 ± 235.10	6374.00 ± 123.68**	<.001
SIPH[c]	498.40 ± 49.37	185.60 ± 30.05**	<.001
PEAK SI TIME[d]	1.10 ± 0.22	2.20 ± 0.27**	<.001

Note: Group C: Rats intraperitoneally injected with sterile saline. Group PDN: Rats intraperitoneally injected with streptozotocin. Values were presented as mean ± SD. Pre-injection: the SI before Gadolinium-diethylenetriamine Penta-acetic acid (Gd-DTPA) injection.

[a]The peak of SI.

[b]The SI six hours after finishing the Gd-DTPA injection.

[c]The variation of the SI per hour after SI reached its peak.

[d]The time to reach PEAK SI.

**$p < .001$ compared with values in Group C.

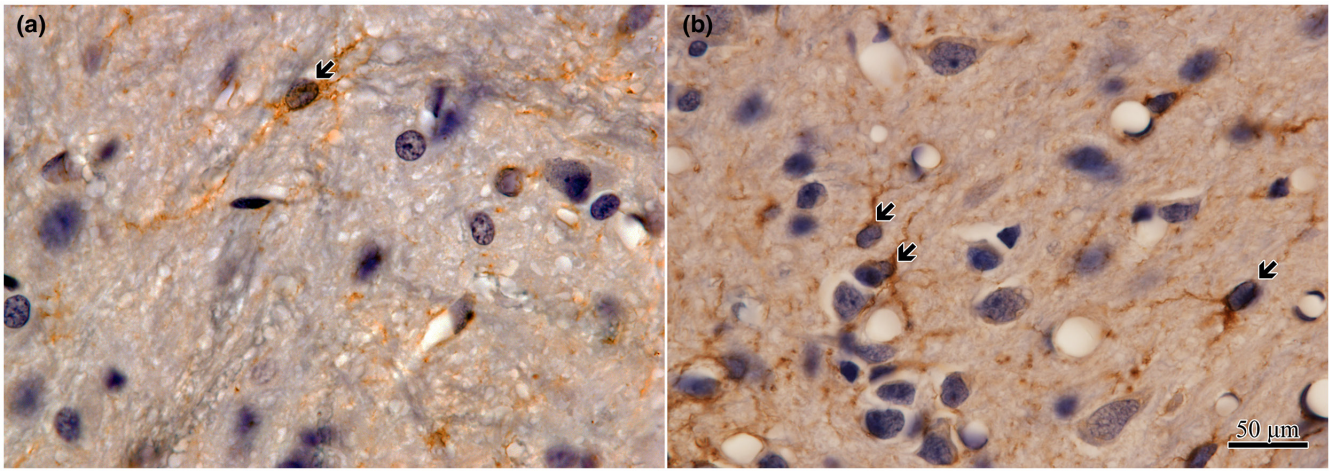

FIGURE 3 Immunostaining of sections, using anti-glial fibrillary acidic protein (GFAP) antibody, obtained from the L5 segment of the spinal cord in the control rats (a) and the PDN rats (b) at 28 days after modeling. ↙: Astrocyte in the lumbar 5 spinal dorsal horn. Astrocytes were identified as GFAP-positive particles.

TABLE 3 Morphometric results obtained from the spinal cord

	Group C ($n = 5$)	Group PDN ($n = 6$)	p-value
Cross-sectional area of the spinal dorsal horn (mm^2)	0.43 ± 0.09	0.44 ± 0.05	.82
No. (103) of astrocytes in the spinal dorsal horn	30.28 ± 4.29	45.51 ± 9.60*	.01
AQP4[a] polarization (%)	66.87 ± 6.90	34.61 ± 6.99**	<.001

Note: See Table 1 for the meaning of the grouping abbreviation. Values were presented as mean ± SD.

[a]Aquaporin-4.

*$p < .05$ compared with values in Group C.; **$p < .001$ compared with values in Group C.

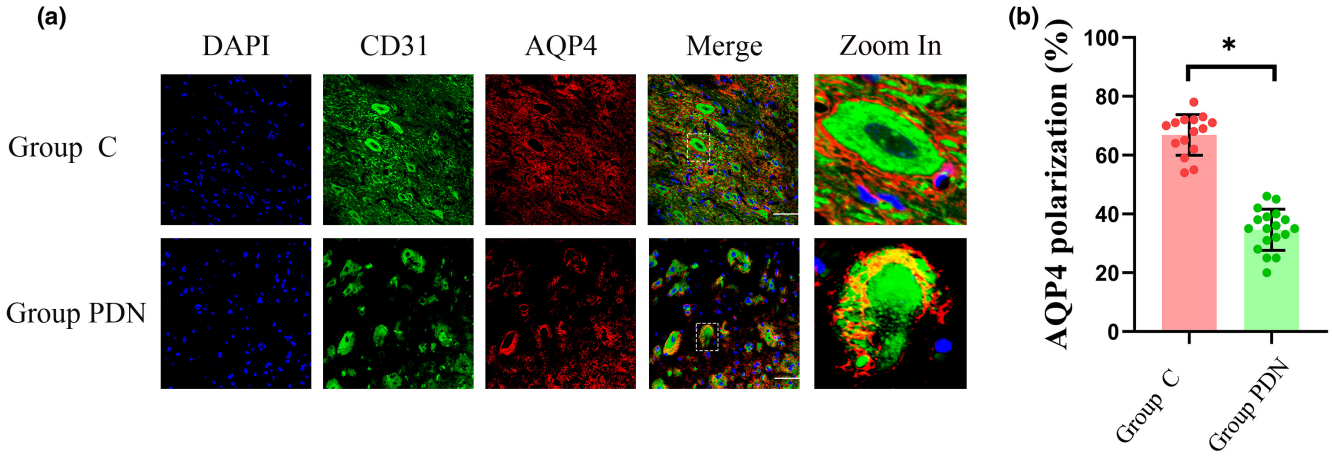

FIGURE 4 Immunofluorescence results. (a) Immunofluorescence staining of sections, using anti-CD31 and anti-AQP4 antibodies, was obtained from the L5 segment of the spinal cord of rats in group C and group PDN. See Figure 1 for the meaning of the grouping abbreviation. AQP4-positive cells were identified with red fluorescence, CD31-positive cells were identified with green fluorescence, the nuclei were counterstained with DAPI (blue). A typical part of AQP4 protein polarity reversal was zoomed in and shown in detail. Scale bar = 50 μm. (b) Quantification of AQP4 polarization similarly demonstrated reduced polarization in blood vessels of rats in the group PDN. Values were presented as mean ± SD. *$p < .05$ compared with values in group C.

with PDN includes deceased contrast infiltration and clearance in the spinal glymphatic system, enhanced mechanical allodynia, increased number of GFAP-positive astrocytes, and reversed polarity of AQP4 protein. All the above characters indicated that there might be a correlation between the impaired spinal glymphatic system and PDN rats.

The glymphatic system is recently discovered as the excretion pathway for metabolic waste products of the central nervous system (Plog & Nedergaard, 2018; Reeves et al., 2020). Many other studies have shown that the glymphatic system also exists in the spinal cord (Benveniste et al., 2017; Liu et al., 2018; Wei et al., 2017). MRI has been widely used to study the functional variation of the glymphatic system due to its great potential for sensitive and non-invasive evaluation of the exchange of cerebrospinal fluid (CSF) with interstitial fluid (ISF) (Gakuba et al., 2018; Jiang, 2019; Zhang et al., 2019). So based on the above pieces of evidence, we injected Gd-DTPA into the L4/5 subarachnoid space on living rats with PDN and evaluated the infiltration and clearance of the contrast agent for indicating the functional variation of the spinal glymphatic system. Using MRI evaluation, we have found a deceased clearance of contrast agent in the spinal glymphatic system on the living rats with PDN, which indicated that the activity of the spinal glymphatic system in PDN rats was impaired.

Cognitive deficits have been manifested to be associated with the impairment of the glymphatic system of the brain in type-2 diabetes mellitus rats (Jiang et al., 2017). And few studies have investigated the correlation between the spinal glymphatic system and PDN. This is the first study injecting Gd-DTPA into the L4/5 subarachnoid space and using MRI scanning to determine the functional variation of the glymphatic system during the process of PDN. After Gd-DTPA injection, there was no contrast agent signal in white matter, which may be related to the white matter tracts being dense so that the contrast agent was not easy to inflow into the interstitial space (Wei et al., 2017). As shown in this study, 15 min after Gd-DTPA injection, the contrast agent was discontinuously distributed on the surface of the pia mater, which may be related to the perforating arteries of the pia mater surface penetrating into the spinal cord radially. The contrast agent inflowed into the ventral horn and the dorsal horn along the anterior lateral sulcus or posterior-lateral sulcus, which may be related to the branches of radicle arteries penetrating into the spinal cord along the anterior lateral sulcus and posterior-lateral sulcus. The above results showed that the contrast agent may be inflowed into the spinal cord along with the perivascular space of the radicle arteries and the perforating arteries of the pia mater, and due to the limits of the concentration and injection speed of Gd-DTPA, we did not find clear evidence to prove that process, and we hope to figure it out in the future study.

In this study, there was no difference in the PEAK SI between groups, the PEAK SI TIME prolonged and SIX-HOUR SI increased significantly in the PDN group, and the SIPH decreased significantly in the PDN group. The inflowing of contrast agent into the spinal parenchyma was a time-dependent process. The inflowing and removal of contrast agent in spinal parenchyma were carried out simultaneously (Wei et al., 2017). During the first hour post-infusion, the contrast agent influx outweighed its clearance in control animals. One and a half hours post-infusion, the clearance of the contrast agent outweighed its influx in Group C. However, during the 2-h post-infusion, the contrast agent influx still outweighed its clearance, and 2.5-h post-infusion, the contrast agent clearance outweighed its influx in the Group PDN. These results showed that the infiltration and clearance of the contrast agent in the spinal cord of PDN rats were significantly deceased than the non-PDN rats, which may be related to the CSF bulk speed in the para-vasculature network was lower in the spinal cord of PDN rats (Davoodi-Bojd et al., 2019). Previous studies have shown that diabetes alters the arteriolar structure and increases the perivascular space (Jiang et al., 2017). Hyperglycemia is related to the formation of free radicals including advanced glycation end products and to an increase in inflammatory processes (Miranda et al., 2019). Inflammation may also enlarge the perivascular space. The enlarged perivascular space which leads to stagnant glymphatic transport could be one factor for deceased clearance of contrast agent in the spinal cord of PDN rats (Kress et al., 2014; Peng et al., 2016). The activity and efficiency of the glymphatic system of the spinal cord were impaired in PDN rats.

Astrocytes were considered as the important structural foundation of the glymphatic system (Plog & Nedergaard, 2018). Previous studies have indicated that chronic neuropathic pain might result from dysfunctional, chronically "over-activated astrocytes" (Nesic et al., 2005). It was reported that astrocyte activation contributed to mechanical allodynia in a mouse model of type 2 diabetes (Liao et al., 2010). In the present study, we applied stereology techniques and found out that the number of GFAP-positive astrocytes increased significantly in the spinal dorsal horn of PDN rats. Our results added new evidence of numerical plasticity of GFAP-positive astrocytes to the process of PDN which indicated that the GFAP-positive astrocytes were not only dysfunctionally overactivated but also numerically increased. This plasticity of GFAP-positive astrocytes might contribute to the impaired glymphatic system of the spinal cord.

The glymphatic system is composed of periarterial space, perivenous space, and AQP4 which is specifically localized to perivascular astrocytic end foot processes (Iliff et al., 2012; Liu et al., 2018). AQP4 is a water channel predominantly expressed within astrocytic processes that form the subpial and subependymal glial-limiting membranes and within the perivascular astrocytic end foot processes that circumscribe the entirety of the cerebrovasculature (Plog & Nedergaard, 2018). It has been discovered that the density of AQP4 is greatest in the region of the astrocytic end foot processes closest to the vessel (also known as the polarized expression of AQP4) under normal conditions. Loss of AQP4 polarity refers to AQP4 expression being mislocalized and broadly distributed in astrocytes, rather than being focused on the end foot surrounding blood vessels. Due to its particularly high expression at the blood–brain barrier (BBB) and blood–CSF barrier, AQP4 plays an important role in the CSF-ISF (interstitial fluid) exchange and the removal of waste solutes in ISF (Benveniste et al., 2017; Mader & Brimberg, 2019). Many neurological conditions are now found to be associated with an alteration in AQP4 localization. Emerging pieces of evidence indicate that reversed AQP4 polarity is involved in the disturbed blood–brain barrier, regulation of extracellular space (ECS) volume and potassium homeostasis, epilepsy, stroke, and edema (Hubbard et al., 2018; Lu, Zhan, et al., 2020; Nagelhus & Ottersen, 2013; Wolburg et al., 2012).

In the present study, AQP4 protein expression was not highly located in perivascular end foot processes, AQP4 'polarization' significantly reduced when compared with Group C. After the three channels in Figure 4 were merged, it was obvious that in the PDN group, red AQP4 was not closely distributed around the cross section of blood vessels, but discontinuous, and there was even no AQP4 distribution in some perivascular regions, indicating that the polarity of AQP4 had changed significantly in the Group PDN. Besides, we also noticed that there were seemed to have some differences in the architecture such as the blood vessels between the control group and the PDN group in Figure 4, and it may be related to vascular endothelial dysfunction and atherosclerosis interfered with the binding of CD31. The nonspecific staining motor neurons in the control pictures, which acted like dendrites extending off of the blood vessels, often bind indiscriminately to antibodies (including some secondaries) and may be confused with CD31. To avoid these potential interferences, we only selected perivascular regions with blood vessels that seemed relatively complete and with no dendrites. In the present study, CD31 was only used for the localization of blood vessels and did not participate in the measurement of AQP4 polarity, so it would not interfere with the quantification of AQP4 polarization. Hence, the results of AQP4 polarization in the present study were reliable and believable. Our results manifested the polarity reversal of AQP4 protein in PDN rats, which might result in an impaired spinal glymphatic system.

It should be noted that the increased AQP4 expression and its redistribution/surface localization can be two different concepts. Previous studies have shown an increase in AQP4 membrane localization in primary human astrocytes which is not accompanied by a change in AQP4 protein expression levels, which means the expression and localization variation of AQP4 can be discordant (Salman et al., 2017). This mislocalization can be a potential therapeutic target (Ciappelloni et al., 2019). As well as being crucial for water homeostasis, AQPs are involved in physiologically important transport of molecules other than water, regulation of surface expression of other membrane proteins, cell adhesion, signaling in cell volume regulation, sensory functions, defense and metabolism, and motility and cancer (Kitchen et al., 2015; Wagner et al., 2022). Moreover, a subgroup of AQP water channels also facilitates transmembrane diffusion of small, polar solutes (Kitchen et al., 2019). It was reported that the targeted modulation of AQPs presents an opportunity to

develop novel treatments for diverse conditions and there is no single drug that has yet been approved to successfully target it due to the complex communications between AQPs (mainly AQP4) and other therapeutic targets (Abir-Awan et al., 2019; Verkman et al., 2014). The therapeutic effect of AQP4 targeted treatment through the glymphatic system on edema and PDN also needs further research. Regulation of AQPs function by subcellular relocalization is a ubiquitous regulatory mechanism across the mammalian AQP family and recent studies have suggested that targeting the trafficking of AQPs proteins to the plasma membrane is a viable alternative drug target to direct inhibition of the water-conducting pore (Markou et al., 2022). Recent breakthroughs indicate that inhibition of hydrogen peroxide permeation through AQP1 provides a new approach to treating hypertrophic cardiomyopathies and inhibition of AQP4 localization with the licensed drug trifluoperazine provides compelling evidence for a new approach to treating CNS edema (Salman, Kitchen, Yool, et al., 2022). The discovery and development of small-molecule AQP inhibitors for research use and therapeutic development will lead to new insights into the basic biology of and novel treatments for the wide range of AQP-associated disorders (Wagner et al., 2022). The AQP4 protein expression in PDN rats also needs further research.

In this study, the intrathecal injection rate of tracer into the CSF may disturb the regular CSF flow. In addition, it evoked an increased MRI signal-to-noise ratio of the lumbar enlargement of the spinal cord to better detect impairment of the glymphatic system and provide more reliable data for quantitative analysis (Ding et al., 2018). Moreover, we used the classic MRI tracer, the Gd-DTPA, to investigate the functional variations of paracellular flow of the spinal glymphatic system. The classic tracer studies measure this paracellular flow based on an directly dependent AQP4, while the use of H217O captures both paracellular flow and diffusive transcellular exchange of water based on an indirectly dependent AQP4 (Salman et al., 2021). More studies are needed to investigate the use of H217O to detect functional changes in the spinal glymphatic system of PDN rats. Previous studies have demonstrated that anesthesia with isoflurane reduces glymphatic function, especially in glymphatic influx and long-term isoflurane anesthesia does not affect overall glymphatic function (Hablitz et al., 2019). In the present study, we mainly observed the glymphatic efflux and the interference of isoflurane on glymphatic influx function might be counteracted by long-term isoflurane anesthesia. Of course, the effect of isoflurane anesthesia on the spinal glymphatic system in PDN rats needs further study. MRI scanning was not performed for a longer time due to the limitation of using time of the equipment. So, there was no further comparison of the complete clearance time to contrast agent between no-PDN rats and PDN rats. The pathway of the spinal glymphatic system and its correlations with PDN rats also need further exploration in future studies. In addition, to excluded gender effects, only male SD rats were included in this study, so whether female SD rats also have similar changes needs further studies. Due to the limited funds, we could only establish a type 2 diabetes model based on previous literatures with no measurement of insulin resistance. The difference of the spinal glymphatic system between type 1 and type 2 diabetes also remains to be further studied.

In summary, this study used low-dose STZ intraperitoneal injection combined with a high-fat and high-glucose diet to establish PDN rats with pathophysiological similarity to human type 2 diabetes mellitus successfully. We demonstrated that the activity of the spinal glymphatic system of PDN rats was impaired. Deceased contrast infiltration and clearance, enhanced mechanical allodynia, increased number of GFAP-positive astrocytes, and reversed polarity of AQP4 protein were found in the PDN rats. The above molecular level changes may contribute to the impairment of the spinal glymphatic system in PDN rats. This study revealed the molecular and functional variations of the spinal glymphatic system in PDN rats and for the first time indicated that there might be a correlation between the impaired spinal glymphatic system and PDN rats.

AUTHOR CONTRIBUTIONS

Conceptualization, J.L. and G.W. *Methodology*, G.W., F.W., and Y.H.; *Validation*, G.W., F.W., and Y.H.; *Formal Analysis*, G.W., F.W., and Y.H.; *Writing – Original Draft*: F.W.; *Writing – Review & Editing*, J.L. and F.W.; *Supervision*, J.L. and F.W.; *Project Administration*, J.L.; *Funding Acquisition*, J.L.

ACKNOWLEDGMENTS

We thank Tao Cheng (Department of Radiology, North Sichuan Medical College), Guo-Yun Qing, and Tao Xiang (laboratory animal center of North Sichuan Medical College) for their assistance in the laboratory work and animal care.

CONFLICT OF INTEREST

The authors declare that the research was conducted in the absence of any commercial or financial relationships that could be construed as a potential conflict of interest.

PEER REVIEW

The peer review history for this article is available at https://publons.com/publon/10.1002/jnr.25104.

DATA AVAILABILITY STATEMENT

The data that support the findings of this study are available from the corresponding author upon reasonable request.

ORCID

Jing-Yan Lin https://orcid.org/0000-0001-6706-0751

REFERENCES

Abir-Awan, M., Kitchen, P., Salman, M. M., Conner, M. T., Conner, A. C., & Bill, R. M. (2019). Inhibitors of mammalian aquaporin water channels. *International Journal of Molecular Sciences*, *20*(7), 1589. https://doi.org/10.3390/ijms20071589

Albargothy, N. J., Johnston, D. A., MacGregor-Sharp, M., Weller, R. O., Verma, A., Hawkes, C. A., & Carare, R. O. (2018). Convective influx/glymphatic system: Tracers injected into the CSF enter and leave the brain along separate periarterial basement membrane

pathways. *Acta Neuropathologica*, *136*(1), 139–152. https://doi.org/10.1007/s00401-018-1862-7

Alshuhri, M. S., Gallagher, L., Work, L. M., & Holmes, W. M. (2021). Direct imaging of glymphatic transport using H217O MRI. *JCI Insight*, *6*(10), e141159. https://doi.org/10.1172/jci.insight.141159

Benveniste, H., Lee, H., & Volkow, N. D. (2017). The glymphatic pathway: Waste removal from the CNS via cerebrospinal fluid transport. *Neuroscientist*, *23*(5), 454–465. https://doi.org/10.1177/1073858417691030

Carare, R. O., Hawkes, C. A., & Weller, R. O. (2014). Afferent and efferent immunological pathways of the brain. Anatomy, function and failure. *Brain, Behavior, and Immunity*, *36*, 9–14. https://doi.org/10.1016/j.bbi.2013.10.012

Ciappelloni, S., Bouchet, D., Dubourdieu, N., Boué-Grabot, E., Kellermayer, B., Manso, C., Marignier, R., Oliet, S. H. R., Tourdias, T., & Groc, L. (2019). Aquaporin-4 surface trafficking regulates astrocytic process motility and synaptic activity in health and autoimmune disease. *Cell Reports*, *27*(13), 3860–3872.e4. https://doi.org/10.1016/j.celrep.2019.05.097

Davoodi-Bojd, E., Ding, G., Zhang, L., Li, Q., Li, L., Chopp, M., Zhang, Z. G., & Jiang, Q. (2019). Modeling glymphatic system of the brain using MRI. *Neuroimage*, *188*, 616–627. https://doi.org/10.1016/j.neuroimage.2018.12.039

Ding, G., Chopp, M., Li, L., Zhang, L., Davoodi-Bojd, E., Li, Q., Zhang, Z., & Jiang, Q. (2018). MRI investigation of glymphatic responses to Gd-DTPA infusion rates. *Journal of Neuroscience Research*, *96*(12), 1876–1886. https://doi.org/10.1002/jnr.24325

Gakuba, C., Gaberel, T., Goursaud, S., Bourges, J., Di Palma, C., Quenault, A., Martinez de Lizarrondo, S., Vivien, D., & Gauberti, M. (2018). General anesthesia inhibits the activity of the "glymphatic system". *Theranostics*, *8*(3), 710–722. https://doi.org/10.7150/thno.19154

Galer, B. S., Gianas, A., & Jensen, M. P. (2000). Painful diabetic polyneuropathy: Epidemiology, pain description, and quality of life. *Diabetes Research and Clinical Practice*, *47*(2), 123–128. https://doi.org/10.1016/s0168-8227(99)00112-6

Gundersen, H. J., Bagger, P., Bendtsen, T. F., Evans, S. M., Korbo, L., Marcussen, N., Møller, A., Nielsen, K., Nyengaard, J. R., & Pakkenberg, B. (1988). The new stereological tools: Disector, fractionator, nucleator and point sampled intercepts and their use in pathological research and diagnosis. *APMIS*, *96*(10), 857–881. https://doi.org/10.1111/j.1699-0463.1988.tb00954.x

Hablitz, L. M., Vinitsky, H. S., Sun, Q., Stæger, F. F., Sigurdsson, B., Mortensen, K. N., Lilius, T. O., & Nedergaard, M. (2019). Increased glymphatic influx is correlated with high EEG delta power and low heart rate in mice under anesthesia. *Science Advances*, *5*(2), eaav5447. https://doi.org/10.1126/sciadv.aav5447

Harrison, I. F., Ismail, O., Machhada, A., Colgan, N., Ohene, Y., Nahavandi, P., Ahmed, Z., Fisher, A., Meftah, S., Murray, T. K., Ottersen, O. P., Nagelhus, E. A., O'Neill, M. J., Wells, J. A., & Lythgoe, M. F. (2020). Impaired glymphatic function and clearance of tau in an Alzheimer's disease model. *Brain*, *143*(8), 2576–2593. https://doi.org/10.1093/brain/awaa179

Huang, W., Man, Y., Gao, C., Zhou, L., Gu, J., Xu, H., Wan, Q., Long, Y., Chai, L., Xu, Y., & Xu, Y. (2020). Short-chain fatty acids ameliorate diabetic nephropathy via GPR43-mediated inhibition of oxidative stress and NF-κB signaling. *Oxidative Medicine and Cellular Longevity*, *21*, 4074832. https://doi.org/10.1155/2020/4074832

Hubbard, J. A., Szu, J. I., & Binder, D. K. (2018). The role of aquaporin-4 in synaptic plasticity, memory and disease. *Brain Research Bulletin*, *136*, 118–129. https://doi.org/10.1016/j.brainresbull.2017.02.011

Hussain, N., & Adrian, T. E. (2017). Diabetic neuropathy: Update on pathophysiological mechanism and the possible involvement of glutamate pathways. *Current Diabetes Reviews*, *13*, 488–497. https://doi.org/10.2174/1573399812666160624122605

Iliff, J. J., Lee, H., Yu, M., Feng, T., Logan, J., Nedergaard, M., & Benveniste, H. (2013). Brain-wide pathway for waste clearance captured by contrast-enhanced MRI. *Journal of Clinical Investigation*, *123*(3), 1299–1309. https://doi.org/10.1172/JCI67677

Iliff, J. J., Wang, M., Liao, Y., Plogg, B. A., Peng, W., Gundersen, G. A., Benveniste, H., Vates, G. E., Deane, R., Goldman, S. A., Nagelhus, E. A., & Nedergaard, M. (2012). A paravascular pathway facilitates CSF flow through the brain parenchyma and the clearance of interstitial solutes, including amyloid β. *Science Translational Medicine*, *4*(147), 147ra111. https://doi.org/10.1126/scitranslmed.3003748

Iorio, R., Damato, V., Evoli, A., Gessi, M., Gaudino, S., di Lazzaro, V., Spagni, G., Sluijs, J. A., & Hol, E. M. (2018). Clinical and immunological characteristics of the spectrum of GFAP autoimmunity: A case series of 22 patients. *Journal of Neurology, Neurosurgery, and Psychiatry*, *89*(2), 138–146. https://doi.org/10.1136/jnnp-2017-316583

Iqbal, Z., Azmi, S., Yadav, R., Ferdousi, M., Kumar, M., Cuthbertson, D. J., Lim, J., Malik, R. A., & Alam, U. (2018). Diabetic peripheral neuropathy: Epidemiology, diagnosis, and pharmacotherapy. *Clinical Therapeutics*, *40*(6), 828–849. https://doi.org/10.1016/j.clinthera.2018.04.001

Javed, S., Petropoulos, I. N., Alam, U., & Malik, R. A. (2015). Treatment of painful diabetic neuropathy. *Therapeutic Advances in Chronic Disease*, *6*(1), 15–28. https://doi.org/10.1177/2040622314552071

Jessen, N. A., Munk, A. S., Lundgaard, I., & Nedergaard, M. (2015). The glymphatic system: A Beginner's guide. *Neurochemical Research*, *40*(12), 2583–2599. https://doi.org/10.1007/s11064-015-1581-6

Jiang, Q. (2019). MRI and glymphatic system. *Stroke and Vascular Neurology*, *4*(2), 75–77. https://doi.org/10.1136/svn-2018-000197

Jiang, Q., Zhang, L., Ding, G., Davoodi-Bojd, E., Li, Q., Li, L., Sadry, N., Nedergaard, M., Chopp, M., & Zhang, Z. (2017). Impairment of the glymphatic system after diabetes. *Journal of Cerebral Blood Flow and Metabolism*, *37*(4), 1326–1337. https://doi.org/10.1177/0271678X16654702

Jing-Yan, L. I. N., Bin, P., Yang, Z., & Su, M. (2010). Effects of paraffin embedding and section-sta ining on contractin coefficient of spinal cord in rats. *Journal of Chongqing Medical University*, *35*(12), 1856–1858. https://doi.org/10.13406/j.cnki.cyxb.2010.12.005

Kitchen, P., Day, R. E., Salman, M. M., Conner, M. T., Bill, R. M., & Conner, A. C. (2015). Beyond water homeostasis: Diverse functional roles of mammalian aquaporins. *Biochimica et Biophysica Acta*, *1850*(12), 2410–2421. https://doi.org/10.1016/j.bbagen.2015.08.023

Kitchen, P., Salman, M. M., Halsey, A. M., Clarke-Bland, C., MacDonald, J. A., Ishida, H., Vogel, H. J., Almutiri, S., Logan, A., Kreida, S., al-Jubair, T., Winkel Missel, J., Gourdon, P., Törnroth-Horsefield, S., Conner, M. T., Ahmed, Z., Conner, A. C., & Bill, R. M. (2020). Targeting aquaporin-4 subcellular localization to treat central nervous system edema. *Cell*, *181*(4), 784–799.e19. https://doi.org/10.1016/j.cell.2020.03.037

Kitchen, P., Salman, M. M., Pickel, S. U., Jennings, J., Törnroth-Horsefield, S., Conner, M. T., Bill, R. M., & Conner, A. C. (2019). Water channel pore size determines exclusion properties but not solute selectivity. *Scientific Reports*, *9*(1), 20369. https://doi.org/10.1038/s41598-019-56814-z

Kress, B. T., Iliff, J. J., Xia, M., Wang, M., Wei, H. S., Zeppenfeld, D., Xie, L., Kang, H., Xu, Q., Liew, J. A., Plog, B. A., Ding, F., Deane, R., & Nedergaard, M. (2014). Impairment of paravascular clearance pathways in the aging brain. *Annals of Neurology*, *76*(6), 845–861. https://doi.org/10.1002/ana.24271

Lam, M. A., Hemley, S. J., Najafi, E., Vella, N. G. F., Bilston, L. E., & Stoodley, M. A. (2017). The ultrastructure of spinal cord perivascular spaces: Implications for the circulation of cerebrospinal fluid. *Scientific Reports*, *7*(1), 12924. https://doi.org/10.1038/s41598-017-13455-4

Liao, Y. H., Zhang, G. H., Jia, D., Wang, P., Qian, N. S., He, F., Zeng, X. T., He, Y., Yang, Y. L., Cao, D. Y., Zhang, Y., Wang, D. S., Tao, K. S., Gao, C. J., & Dou, K. F. (2010). Spinal astrocytic activation contributes

to mechanical allodynia in a mouse model of type 2 diabetes. *Brain Research*, *1368*, 324–335. https://doi.org/10.1016/j.brainres.2010.10.044

Lin, J. Y., He, Y. N., Zhu, N., & Peng, B. (2018). Metformin attenuates increase of synaptic number in the rat spinal dorsal horn with painful diabetic neuropathy induced by type 2 diabetes: A stereological study. *Neurochemical Research*, *43*(12), 2232–2239. https://doi.org/10.1007/s11064-018-2642-4

Lin, J. Y., Huang, X. L., Chen, J., Yang, Z. W., Lin, J., Huang, S., & Peng, B. (2017). Stereological study on the number of synapses in the rat spinal dorsal horn with painful diabetic neuropathy induced by streptozotocin. *Neuroreport*, *28*(6), 319–324. https://doi.org/10.1097/WNR.0000000000000762

Liu, S., Lam, M. A., Sial, A., Hemley, S. J., Bilston, L. E., & Stoodley, M. A. (2018). Fluid outflow in the rat spinal cord: The role of perivascular and paravascular pathways. *Fluids Barriers CNS*, *15*(1), 13. https://doi.org/10.1186/s12987-018-0098-1

Liu, Y., Deng, J., & Fan, D. (2019). Ginsenoside Rk3 ameliorates high-fat-diet/streptozocin induced type 2 diabetes mellitus in mice via the AMPK/Akt signaling pathway. *Food & Function*, *22*(5), 2538–2551. https://doi.org/10.1039/c9fo00095j

Lu, G., Pang, C., Chen, Y., Wu, N., & Li, J. (2020). Aquaporin 4 is involved in chronic pain but not acute pain. *Behavioural Brain Research*, *393*, 112810. https://doi.org/10.1016/j.bbr.2020.112810

Lu, H., Zhan, Y., Ai, L., Chen, H., & Chen, J. (2020). AQP4-siRNA alleviates traumatic brain edema by altering post-traumatic AQP4 polarity reversal in TBI rats. *Journal of Clinical Neuroscience*, *81*, 113–119. https://doi.org/10.1016/j.jocn.2020.09.015

Mader, S., & Brimberg, L. (2019). Aquaporin-4 water channel in the brain and its implication for health and disease. *Cell*, *8*(2), 90. https://doi.org/10.3390/cells8020090

Mai, C. L., Tan, Z., Xu, Y. N., Zhang, J. J., Huang, Z. H., Wang, D., Zhang, H., Gui, W. S., Zhang, J., Lin, Z. J., Meng, Y. T., Wei, X., Jie, Y. T., Grace, P. M., Wu, L. J., Zhou, L. J., & Liu, X. G. (2021). CXCL12-mediated monocyte transmigration into brain perivascular space leads to neuroinflammation and memory deficit in neuropathic pain. *Theranostics*, *11*(3), 1059–1078. https://doi.org/10.7150/thno.44364

Markou, A., Unger, L., Abir-Awan, M., Saadallah, A., Halsey, A., Balklava, Z., Conner, M., Törnroth-Horsefield, S., Greenhill, S. D., Conner, A., Bill, R. M., Salman, M. M., & Kitchen, P. (2022). Molecular mechanisms governing aquaporin relocalisation. *Biochimica et Biophysica Acta - Biomembranes*, *1864*(4), 183853. https://doi.org/10.1016/j.bbamem.2021.183853

Mei, X. P., Zhou, Y., Wang, W., Tang, J., Wang, W., Zhang, H., Xu, L. X., & Li, Y. Q. (2011). Ketamine depresses toll-like receptor 3 signaling in spinal microglia in a rat model of neuropathic pain. *Neuro-Signals*, *19*(1), 44–53. https://doi.org/10.1159/000324293

Miranda Pedroso, T. F., Da Bonamigo, T. R., Da Silva, J., Vasconcelos, P., Félix, J. M., Cardoso, C. A. L., Souza, R. I. C., Dos Santos, A. C., Volobuff, C. R. F., Formagio, A. S. N., & Trichez, V. D. K. (2019). Chemical constituents of *Cochlospermum regium* (Schrank) Pilg. Root and its antioxidant, antidiabetic, antiglycation, and anticholinesterase effects in Wistar rats. *Biomedicine & Pharmacotherapy*, *111*, 1383–1392. https://doi.org/10.1016/j.biopha.2019.01.005

Nagelhus, E. A., & Ottersen, O. P. (2013). Physiological roles of aquaporin-4 in brain. *Physiological Reviews*, *93*(4), 1543–1562. https://doi.org/10.1152/physrev.00011.2013

Nesic, O., Lee, J., Johnson, K. M., Ye, Z., Xu, G. Y., Unabia, G. C., Wood, T. G., McAdoo, D. J., Westlund, K. N., Hulsebosch, C. E., & Regino Perez-Polo, J. (2005). Transcriptional profiling of spinal cord injury-induced central neuropathic pain. *Journal of Neurochemistry*, *95*(4), 998–1014. https://doi.org/10.1111/j.1471-4159.2005.03462.x

Peng, B., Lin, J. Y., Shang, Y., Yang, Z. W., & Wang, Y. P. (2010). Plasticity in the synaptic number associated with neuropathic pain in the rat spinal dorsal horn: A stereological study. *Neuroscience Letters*, *486*(1), 24–28. https://doi.org/10.1016/j.neulet.2010.09.037

Peng, W., Achariyar, T. M., Li, B., Liao, Y., Mestre, H., Hitomi, E., Regan, S., Kasper, T., Peng, S., Ding, F., Benveniste, H., Nedergaard, M., & Deane, R. (2016). Suppression of glymphatic fluid transport in a mouse model of Alzheimer's disease. *Neurobiology of Disease*, *93*, 215–225. https://doi.org/10.1016/j.nbd.2016.05.015

Plog, B. A., & Nedergaard, M. (2018). The glymphatic system in central nervous system health and disease: Past, present, and future. *Annual Review of Pathology*, *13*, 379–394. https://doi.org/10.1146/annurev-pathol-051217-111018

Reeves, B. C., Karimy, J. K., Kundishora, A. J., Mestre, H., Cerci, H. M., Matouk, C., Alper, S. L., Lundgaard, I., Nedergaard, M., & Kahle, K. T. (2020). Glymphatic system impairment in Alzheimer's disease and idiopathic Normal pressure hydrocephalus. *Trends in Molecular Medicine*, *26*(3), 285–295. https://doi.org/10.1016/j.molmed.2019.11.008

Rendra, E., Riabov, V., Mossel, D. M., Sevastyanova, T., Harmsen, M. C., & Kzhyshkowska, J. (2019). Reactive oxygen species (ROS) in macrophage activation and function in diabetes. *Immunobiology*, *224*(2), 242–253. https://doi.org/10.1016/j.imbio.2018.11.010

Rivera-Aponte, D. E., Méndez-González, M. P., Rivera-Pagán, A. F., Kucheryavykh, Y. V., Kucheryavykh, L. Y., Skatchkov, S. N., & Eaton, M. J. (2015). Hyperglycemia reduces functional expression of astrocytic Kir4.1 channels and glial glutamate uptake. *Neuroscience*, *310*, 216–223. https://doi.org/10.1016/j.neuroscience.2015.09.044

Salman, M. M., Kitchen, P., Halsey, A., Wang, M. X., Törnroth-Horsefield, S., Conner, A. C., Badaut, J., Iliff, J. J., & Bill, R. M. (2022). Emerging roles for dynamic aquaporin-4 subcellular relocalization in CNS water homeostasis. *Brain*, *145*, 64–75. https://doi.org/10.1093/brain/awab311

Salman, M. M., Kitchen, P., Iliff, J. J., & Bill, R. M. (2021). Aquaporin 4 and glymphatic flow have central roles in brain fluid homeostasis. *Nature Reviews Neuroscience*, *22*(10), 650–651. https://doi.org/10.1038/s41583-021-00514-z

Salman, M. M., Kitchen, P., Woodroofe, M. N., Brown, J. E., Bill, R. M., Conner, A. C., & Conner, M. T. (2017). Hypothermia increases aquaporin 4 (AQP4) plasma membrane abundance in human primary cortical astrocytes via a calcium/transient receptor potential vanilloid 4 (TRPV4)- and calmodulin-mediated mechanism. *European Journal of Neuroscience*, *46*(9), 2542–2547. https://doi.org/10.1111/ejn.13723

Salman, M. M., Kitchen, P., Yool, A. J., & Bill, R. M. (2022). Recent breakthroughs and future directions in drugging aquaporins. *Trends in Pharmacological Sciences*, *43*(1), 30–42. https://doi.org/10.1016/j.tips.2021.10.009

Schmader, K. E. (2002). Epidemiology and impact on quality of life of postherpetic neuralgia and painful diabetic neuropathy. *Clinical Journal of Pain*, *18*, 350–354. https://doi.org/10.1097/00002508-200211000-00002

Schreiber, A. K., Nones, C. F., Reis, R. C., Chichorro, J. G., & Cunha, J. M. (2015). Diabetic neuropathic pain: Physiopathology and treatment. *World Journal of Diabetes*, *6*(3), 432–444. https://doi.org/10.4239/wjd.v6.i3.432

Stokum, J. A., Mehta, R. I., Ivanova, S., Yu, E., Gerzanich, V., & Simard, J. M. (2015). Heterogeneity of aquaporin-4 localization and expression after focal cerebral ischemia underlies differences in white versus grey matter swelling. *Acta Neuropathologica Communications*, *3*, 61. https://doi.org/10.1186/s40478-015-0239-6

Sylvain, N. J., Salman, M. M., Pushie, M. J., Hou, H., Meher, V., Herlo, R., Peeling, L., & Kelly, M. E. (2021). The effects of trifluoperazine on brain edema, aquaporin-4 expression and metabolic markers during the acute phase of stroke using photothrombotic mouse model. *Biochimica et Biophysica Acta - Biomembranes*, *1863*(5), 183573. https://doi.org/10.1016/j.bbamem.2021.183573

Verkman, A. S., Anderson, M. O., & Papadopoulos, M. C. (2014). Aquaporins: Important but elusive drug targets. *Nature Reviews Drug Discovery*, *13*(4), 259–277. https://doi.org/10.1038/nrd4226

Wagner, K., Unger, L., Salman, M. M., Kitchen, P., Bill, R. M., & Yool, A. J. (2022). Signaling mechanisms and pharmacological modulators

governing diverse aquaporin functions in human health and disease. *International Journal of Molecular Sciences*, *23*(3), 1388. https://doi.org/10.3390/ijms23031388

Wei, F., Zhang, C., Xue, R., Shan, L., Gong, S., Wang, G., Tao, J., Xu, G., Zhang, G., & Wang, L. (2017). The pathway of subarachnoid CSF moving into the spinal parenchyma and the role of astrocytic aquaporin-4 in this process. *Life Sciences*, *182*, 29–40. https://doi.org/10.1016/j.lfs.2017.05.028

Wolburg, H., Noell, S., Fallier-Becker, P., Mack, A. F., & Wolburg-Buchholz, K. (2012). The disturbed blood-brain barrier in human glioblastoma. *Molecular Aspects of Medicine*, *33*(5–6), 579–589. https://doi.org/10.1016/j.mam.2012.02.003

Wood, A. K., Klide, A. M., Pickup, S., & Kundel, H. L. (2001). Prolonged general anesthesia in MR studies of rats. *Academic Radiology*, *8*(11), 1136–1140. https://doi.org/10.1016/S1076-6332(03)80727-4

Xu, J. J., Walla, B. C., Diaz, M. F., Fuller, G. N., & Gutstein, H. B. (2006). Intermittent lumbar puncture in rats: A novel method for the experimental study of opioid tolerance. *Anesthesia and Analgesia*, *103*(3), 714–720. https://doi.org/10.1213/01.ane.0000226100.46866.ea

Zhang, J., Liu, Y., Zheng, Y., Luo, Y., Du, Y., Zhao, Y., Guan, J., Zhang, X., & Fu, J. (2020). TREM-2-p38 MAPK signaling regulates neuroinflammation during chronic cerebral hypoperfusion combined with diabetes mellitus. *Journal of Neuroinflammation*, *17*(1), 2. https://doi.org/10.1186/s12974-019-1688-9

Zhang, L., Chopp, M., Jiang, Q., & Zhang, Z. (2019). Role of the glymphatic system in ageing and diabetes mellitus impaired cognitive function. *Stroke and Vascular Neurology*, *4*(2), 90–92. https://doi.org/10.1136/svn-2018-000203

Zhong-Xian, L., Ji-Yong, L., Ji-Heng, C., & Hao-Sheng, B. (2004). Application of percutaneous intrathecal administration in rats in basic research of pain. *Journal of Fujian Medical University*, *38*(2), 185–187.

SUPPORTING INFORMATION

Additional supporting information can be found online in the Supporting Information section at the end of this article.

Transparent Peer Review Report

Transparent Science Questionnaire for Authors

How to cite this article: Wang, G-Q, Wang, F-X, He, Y-N, & Lin, J-Y (2022). Plasticity of the spinal glymphatic system in male SD rats with painful diabetic neuropathy induced by type 2 diabetes mellitus. *Journal of Neuroscience Research*, *100*, 1908–1920. https://doi.org/10.1002/jnr.25104